NANO LETTERS

Letter

pubs.acs.org/NanoLett

Bent Ferroelectric Domain Walls as Reconfigurable Metallic-Like Channels

Igor Stolichnov,*[,†] Ludwig Feigl,[†] Leo J. McGilly,[†] Tomas Sluka,[†,‡] Xian-Kui Wei,[†,§] Enrico Colla,[†] Arnaud Crassous,[†] Konstantin Shapovalov,[†] Petr Yudin,[†] Alexander K. Tagantsev,[†] and Nava Setter[†]

[†]Ceramics Laboratory, EPFL-Swiss Federal Institute of Technology, Lausanne 1015, Switzerland

[‡]DPMC-MaNEP, University of Geneva, 24 Quai Ernest Ansermet, 1211 Geneva 4, Switzerland

[§]Peter Grunberg Institute and Ernst Ruska Center for Microscopy and Spectroscopy with Electrons, Research Center Jülich, Jülich 52425, Germany

Supporting Information

ABSTRACT: Use of ferroelectric domain-walls in future electronics requires that they are stable, rewritable conducting channels. Here we demonstrate nonthermally activated metallic-like conduction in nominally uncharged, bent, rewritable ferroelectric-ferroelastic domain-walls of the ubiquitous ferroelectric $Pb(Zr,Ti)O_3$ using scanning force microscopy down to a temperature of 4 K. New walls created at 4 K by pressure exhibit similar robust and intrinsic conductivity. Atomic resolution electron energy-loss spectroscopy confirms the conductivity confinement at the wall. This work provides a new concept in "domain-wall nanoelectronics".

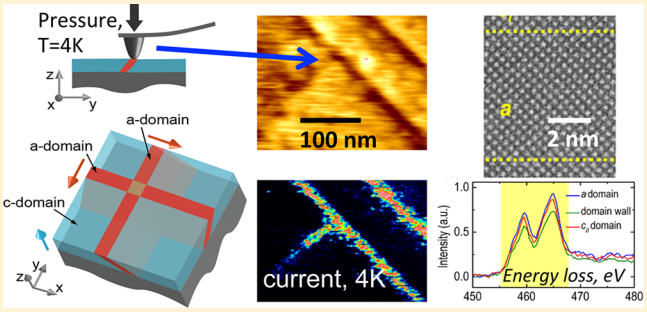

KEYWORDS: *Ferroelectric, domain wall, metallic, scanning probe microscopy*

Electronic transport at domain walls[1−6] or wall/interface junctions,[7] a required cornerstone for domain wall nanoelectronics is difficult to control due to the sensitivity of the conduction to the defect chemistry of the material,[3,8] its strong temperature dependence,[3,4,9] and polarization-related hysteresis effects.[2,10] Furthermore, displaced domain walls leave conductive footprints due to accumulated mobile defects,[11] which questions the feasibility of rewritable domain wall based circuits. Because of these issues, electronic conductivity in domain walls since its first demonstration by Seidel et al.[1] remained elusive with a large dispersion in the reported transport data.[3−5,10,12] Metallic-like conductivity at domain walls was shown only transiently in individually switched nanodomains[13] or in so-called charged domain walls,[14−17] prepared individually using a special poling procedure. Stable metallic-type conduction was so far only shown in the case of strongly charged domain walls.[15,17,18] In strongly charged walls, the polarization continuity is broken with the bound charge at the domain boundary resulting in compensation with a narrow metallic-like conductive layer that may result in nonthermally activated transport.[15] However, the formation energy of charged domain walls is very high.[19] In addition, strong depolarizing fields, inversely proportional to the domain wall spacing, destabilize the walls when they are located in close proximity to each other (e.g., < 1 μm for $BaTiO_3$ crystals).[14]

While strongly charged domain walls might therefore be difficult to implement in electronics, another possibility exists that offers both the high conductivity of charged walls and the positional stability of neutral walls: when neutral ferroelectric domain walls are forced to bend off their neutral position, these nominally uncharged walls inevitably become partly charged and thus may display metallic-like conductivity. The desired stability can be obtained for bent neutral ferroelectric walls that are ferroelastic, as shown below.

Domain walls in bulk ferroelastic crystals acquire elastically compatible orientations. Any deviation of a wall from this equilibrium orientation results in the appearance of elastic fields of amplitude proportional to the rotation angle α, implying an energy increase in the system proportional to α^2 (for details see Supporting Information). In the case of ferroelastic thin films, a lattice mismatch with the substrate produces elastic fields that can be relaxed by the rotation of the walls. The energy release due to this rotation is proportional to the rotation angle α. Therefore, in thin films the stable orientation of ferroelastic walls is tilted off the bulk equilibrium orientation by the angle α which gives the highest overall energy reduction. This implies a possibility to tune the orientation of ferroelectric/ferroelastic walls in thin films via the control of the film/substrate lattice misfit and the configuration of the domain pattern. The higher the rotation angle α, the higher is the charge density in the wall and its conductivity.

We illustrate this for the case of tetragonal a/c domain pattern, where c-domains have their *c*-axis (the polar axis) perpendicular

Received: August 27, 2015
Revised: October 28, 2015
Published: November 10, 2015

DOI: 10.1021/acs.nanolett.5b03450
Nano Lett. 2015, 15, 8049−8055

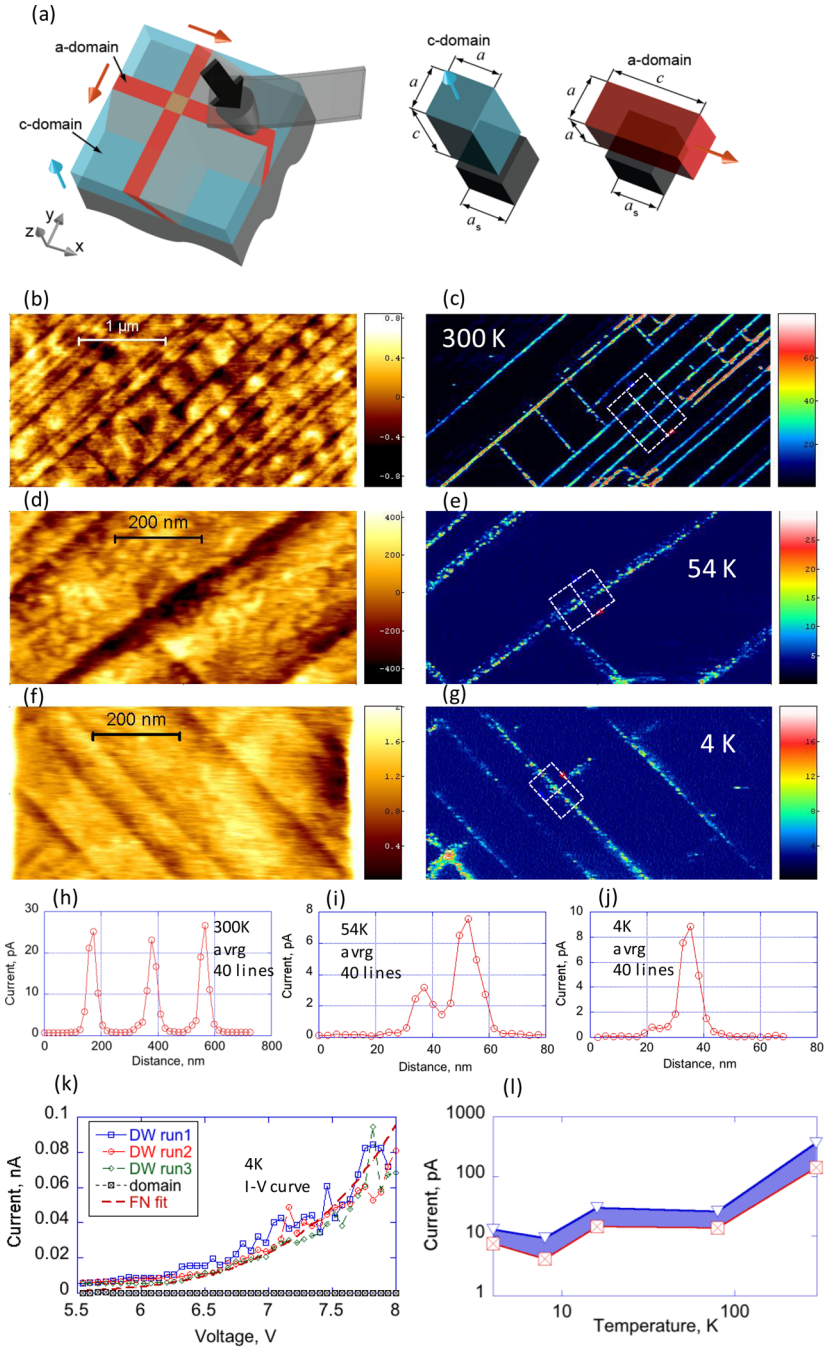

Fig. 1

Figure 1. Conduction along a-domains in 60 nm thick PZT film measured by cAFM. (a) Illustration of the *a*/c-domain pattern in the tetragonal film on the substrate with the AFM tip probing the surface. The *c*-domains (a-domains) have their *c* (*a*) lattice parameter perpendicular to the surface. The color scheme is substrate (dark gray), c-domains (blue), and a-domains (red). Blue and red arrows show the polarization direction for *c*- and a-domains, respectively. (b,c) Topography and conduction map measured at ambient conditions under dc tip bias of −6.5 V. (d,e) Topography and conduction map measured at 54 K under dc tip bias of −7 V. (f,g) Topography and conduction map measured at 4 K under dc tip bias of −7 V. (h−j) Cross sections of the conductive traces averaged over 40 lines measured on the images (c,e,g), respectively. The areas used for the measurements are marked on the corresponding images with white dashed frames. (k) Sequential *I*−*V* curves measured at 4 K using the stationary probe positioned on the conductive trace. The dashed line shows the Fowler−Nordheim fit (see Supporting Information for the fit parameters). (l) Temperature-dependence of domain wall conduction obtained from the cAFM histograms analysis. The color band represents the range of current values defined by the most conductive 5% of the cAFM scan histogram (upper limit) and most conductive 25% (lower limit).

to the surface of the film and a-domains have their *c*-axis in the plane of the film, as illustrated in Figure 1a. We impose a substrate with a lattice constant a_s, which slightly exceeds lattice constant of the ferroelectric a ($a_s - a \ll c - a$ where c is the larger lattice constant of the ferroelectric), implying narrow a-domains.[20] We use a simplified expression for the energy of the system (for a detailed discussion see Supporting Information)

$$\Delta E \approx \frac{A}{2}\alpha^2 - B\frac{a_s - a}{a_s}\alpha - Bf\left(\frac{w}{h}\right)\frac{a_s - c}{a_s}\alpha \qquad (1)$$

DOI: 10.1021/acs.nanolett.5b03450
Nano Lett. 2015, 15, 8049−8055

where A and B are positive constants while w and h are the a-domain width and the film thickness, respectively. Here the first term is the incompatibility energy of the wall. The second and the third terms control the stress release due to the wall rotation. The second term is the wall/c-domain-misfit coupling energy while the third is the coupling energy between the wall and the lattice misfit in the narrow a-domain; the positive function behavior $f(w/h) \rightarrow 0$ once $w/h \rightarrow 0$ (Supporting Information Figure S2) reflects the fact that the interaction with the a-domain vanishes when its width goes to zero. Minimization of eq 1 yields the rotation angle for the wall

$$\alpha = \frac{B}{A}\frac{a_s - a}{a_s} + \frac{B}{A} f\left(\frac{w}{h}\right)\frac{a_s - c}{a_s} \quad (2)$$

In view of the opposite signs of the lattice misfits of the a-domain and c-domain ($a_s - a > 0$, $a_s - c < 0$), eq 2 shows that a reduction in a-domain width (and consequently also reduction of $f(w/h)$) leads to an increase of the rotation angle. This reasoning is oversimplified but its consequence, namely, the increase of the rotation angle upon reduction of the a-domain width, does hold. For the exact details, see Supporting Information.

Thus, to have stable domain walls with nonthermally activated conduction, a highly tetragonal film can be used on a substrate whose lattice parameter is slightly larger than the small lattice parameter of the film. Below we demonstrate experimentally that this concept works.

Highly tetragonal PZT films (Zr/Ti = 10:90) were grown on $DyScO_3$ (DSO) substrate having a small tensile lattice mismatch with respect to the c-domains of the PZT. Twenty nanometers of $SrRuO_3$ bottom electrodes were introduced between DSO and PZT; for further growth and characterization details see Supporting Information. The 60 nm thick PZT film was mainly *c*-oriented having 10 nm wide a-domains (Figure 1a). Ambient conductive atomic force microscope (cAFM) measurements showed stable current traces that closely reproduced the a-domain pattern, Figure 1b,c, in agreement with earlier results[20] where also the expected domain wall bending was clearly observed. Ultrahigh vacuum (UHV) scanning force microscopy using conductive diamond probes (see Supporting Information for further details) showed similar results with clear conduction signal from a-domains. Remarkably the measured conduction at the a-domains showed very weak temperature dependence throughout a wide temperature range from 300 down to 4 K. cAFM scans measured under constant tip bias of −7 V at 54 K (Figure 1e) and 4 K (Figure 1g) are shown with their corresponding topography maps, Figure 1d,f, respectively. The a-domains seen on the topography images are signaled in cAFM scans by clear conduction traces, while the c-domains show no current. The current measured through the cross-section of the conduction line (averaged over 40 lines) at 4 K (Figure 1j) and 54 K (Figure 1i) are similar to each other and comparable with the ambient measurements (Figure 1h). The conduction maps were reproducible and the measured currents did not change significantly when a sequence of maps was taken under identical conditions. The conduction stability was confirmed by sequential $I-V$ measurements using a stationary tip positioned at the a-domain, Figure 1k. These $I-V$ curves could be fitted using Fowler−Nordheim formula with a triangular tunneling barrier of 1.1 eV with parameters close to those used for tunneling though the tip/PZT interface in ref 21 (see Supporting Information for fit details). This means that tunneling injection through the barrier of the tip/PZT interface is the most likely factor that limits the conduction and determines a rather high conduction onset voltage (>5.5 V).

In order to evaluate the temperature dependence of the current we analyzed the histograms of cAFM images collected in UHV at five different temperatures from 300 to 4 K using the same probe. In order to minimize the probe tip change during the series of scans we employed a "nonsharp" tip with the radius >50 nm, which produced rather wide conduction traces of 50−80 nm (see Supporting Information for details). The range of current values defined by the most conductive 5% of the cAFM scan histogram (upper limit) and most conductive 25% (lower limit) are plotted in Figure 1l for different temperatures. The results confirm the trend observed in the cross sections (Figure1h−j): the temperature dependence of current at the domain walls is very weak, in particular within the temperature range of 4−80 K.

All conduction measurements have been carried out at the negative tip bias that did not alter the out-of-plane polarization of the c-domains. In additional experiments, the out-of-plane polarization was reversed locally prior to cAFM map collection. The conductive traces at a-domains were found to be stable and independent of the local change of out-of-plane polarization in c-domains. (See Supporting Information for details.)

To localize the conductivity precisely, we used improved resolution UHV cAFM. Resolution enhancement was reached by using diamond tips at low force of 1−3 nN that preserved the pristine tip sharpness throughout the scans (see Supporting Information for details). The resulting 250 × 250 nm^2 cAFM scans delivered high-resolution conduction maps with clear double conductive lines corresponding to the a-domain boundaries, Figure 2a. The cross-section profiles of the conduction traces averaged over 30 lines show two distinct peaks with half-maximum width of 5 ± 1 nm separated by a low conduction zone in the center of the a-domain, Figure 2b. The distance between the peak maxima is 14 ± 1 nm, which is close to the a-domain width of 10−11 nm measured on an identically prepared sample by transmission electron microscopy (TEM), Figure 2c. The high-resolution cAFM data indicate that the conduction is located at the a-domain boundaries rather than the entire a-domain.

The fine structure of conductive traces in Figure 2 with reproducible conductive spots further confirms the interface-limited electron transport in the studied films (for details see Supporting Information). This structure may originate from variable defect concentration at the interface, which influences the barrier height for electron injection. Thus, the high-resolution cAFM data indicate that the measured current is localized at the boundaries of ultrafine 10−15 nm a-domains, which behave as conductive channels.

To further explore the nature of the conduction, we investigated new a-domains created by pure mechanical force exerted by the AFM tip without application of electrical bias. As confirmed by phase field simulation, (Supporting Information) mechanical force applied by a probing tip on the film surface should create and stabilize an a-domain. Indeed, in the experiment the application of high force >200 nN to the probe tip resulted in formation of new stable transverse a-domains, visible in the subsequent scans (depicted in Figure 3a,b). In the experiment presented in Figure 3c−f cAFM scans were performed twice at 4 K under identical conditions with a tip bias of −7 V. Between the two cAFM measurements, the sample was rescanned with a high force of 250 ± 50 nN applied to the tip, which is significantly higher than the force of 10−20 nN routinely used for cAFM in this study.

DOI: 10.1021/acs.nanolett.5b03450
Nano Lett. 2015, 15, 8049−8055

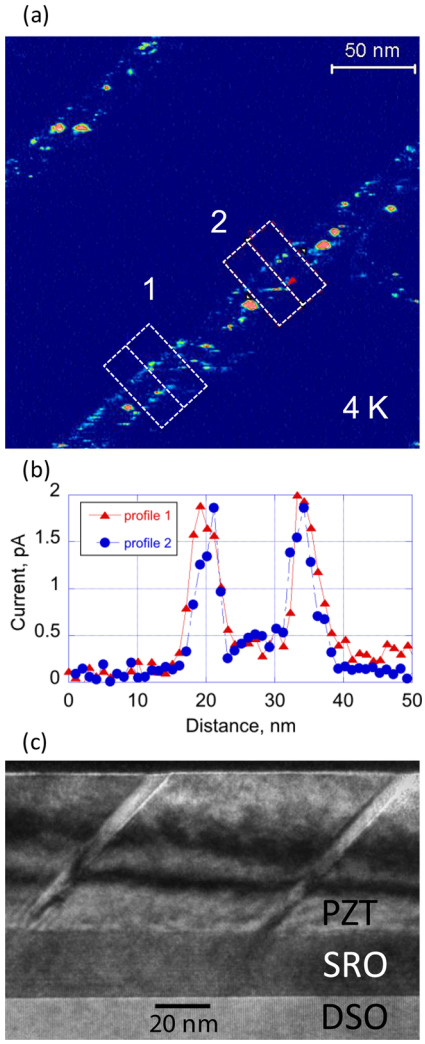

Figure 2. Conduction of individual domain boundaries of ultrafine a-domains resolved by cAFM. (a) Enhanced resolution conduction map measured at 4 K under dc tip bias of −7 V. (b) Cross sections of the conductive traces averaged over 30 lines measured on the marked areas of the conduction map. (c) TEM cross-section of the 60 nm PZT film grown under conditions identical to the measured film.

The freshly created a-domain was oriented perpendicular to the intrinsic a-domains as seen in the topography image, Figure 3e. The new conductive line, which appears only in the second cAFM scan, Figure 3f, corresponds to the newly formed domain and displays similar current magnitudes compared with the other, previously existing, conducting lines. The number of new conductive domains increased with a further increase of the tip force (for details see Supporting Information), however tip degradation that occurred under these conditions resulted in lower lateral resolution and weaker DW current.

The above results show that the transport along the domain boundaries is an intrinsic property that does not depend on extrinsic defect-mediated conduction; at 4 K the charged defects are frozen, therefore they cannot migrate quickly toward the freshly created a-domain boundaries. Furthermore, these new domains are created by local force without application of any external electrical bias, which excludes electric-field-assisted redistribution of the defects. This differs from the transport properties observed so far on neutral domain walls,[43] which were governed by charged defects at domain boundaries.

To further clarify the origin of the conductivity and check the validity of the analytical model, which considers only the ferroelastic behavior of the film, we investigated the problem by phase-field simulations (for details see Supporting Information). The numerical model incorporates the coupling of ferroelectric, ferroelastic, and electronic properties of the film in the thermodynamic equilibrium. Its results confirm the assumptions of the analytical model that ferroelasticity is the dominant factor, which controls the domain wall bending and leads to charging of the a-domain boundaries. Our phase-field simulations yield a pronounced increase of electron concentration at the a-domain boundaries with decreasing a-domain width (Figure 4a). The origin of this effect is a progressive bending of the walls off their mechanically compatible positions (Supporting Information Figure S6). This conclusion is consistent with that of the analytical theory. Additionally, also the orientation and modulus of spontaneous polarization substantially changes inside the a-domains especially in the vicinity of the film/substrate interface. This bending and polarization changes violate charge neutrality of the walls; the polarization vector breaks its neutral head-to-tail continuity and polarization charge is created at the domain wall. In an ideal dielectric approximation, this bound charge produces a local potential drop of >0.8 V at 50 K. For PZT, with band gap of 3.4 eV[22] and nonzero concentration (10^{14} cm^{-3}) of immobile oxygen vacancies providing defect levels at 0.6 eV below the conduction band,[23] the potential drop at the domain wall is sufficient to push the conduction band below the Fermi level. Thus, in thermodynamic equilibrium the conduction band at the a-domain boundaries is filled with free electrons. Figure 4b predicts the presence of nonthermally activated conduction layer at a-domain boundaries with free carrier concentration exceeding 8×10^{19} cm^{-3} at 50 K for 20 nm wide a-domains. The free carrier concentration at domain walls is weakly temperature-dependent, Supporting Information Figure S7, which is in agreement with the nonthermally activated conduction behavior observed experimentally. The band bending at the domain boundaries decreases upon a-domain width increase, resulting in a smaller electron concentration. The conductive layer totally disappears for a-domain width exceeding 70 nm, which may explain why this conductivity was not observed in intensively studied PZT (Zr/Ti = 20:80) on DSO where a-domains are substantially wider.

The phase-field modeling data discussed above suggest that the metallic-like conduction channels degrade at a distance of 5−20 nm from the interface. Thus, the potential barrier between the probe and conductive channel determines the transport properties measured experimentally. Because of this barrier the conduction is limited by either thermoionic or tunneling injection rather than properties of the conductive domain boundary. The pronounced temperature dependence of conduction observed between the room temperature and 80 K can be explained by the significant contribution of thermoionic emission. Below 80 K, the conduction is nonthermally activated and limited by tunneling in agreement with the $I-V$ curve in Figure 1k.

Finally, direct evidence of the expected changes in electronic structure at bent domain walls is provided by unit-cell scale electron energy-loss spectroscopy (EELS). The EELS mapping experiments were carried out on FEI Titan Chemi-STEM instrument operated at 200 kV. The energy resolution measured from full width at half-maximum of the zero-loss peak was 1.8 eV. The energy dispersion was 0.25 eV/pixel and the aperture size for the collection was 5 mm. In order to gain strong EELS signals, the step size was set as 0.6 nm during the spectrum acquisition.

DOI: 10.1021/acs.nanolett.5b03450
Nano Lett. 2015, 15, 8049−8055

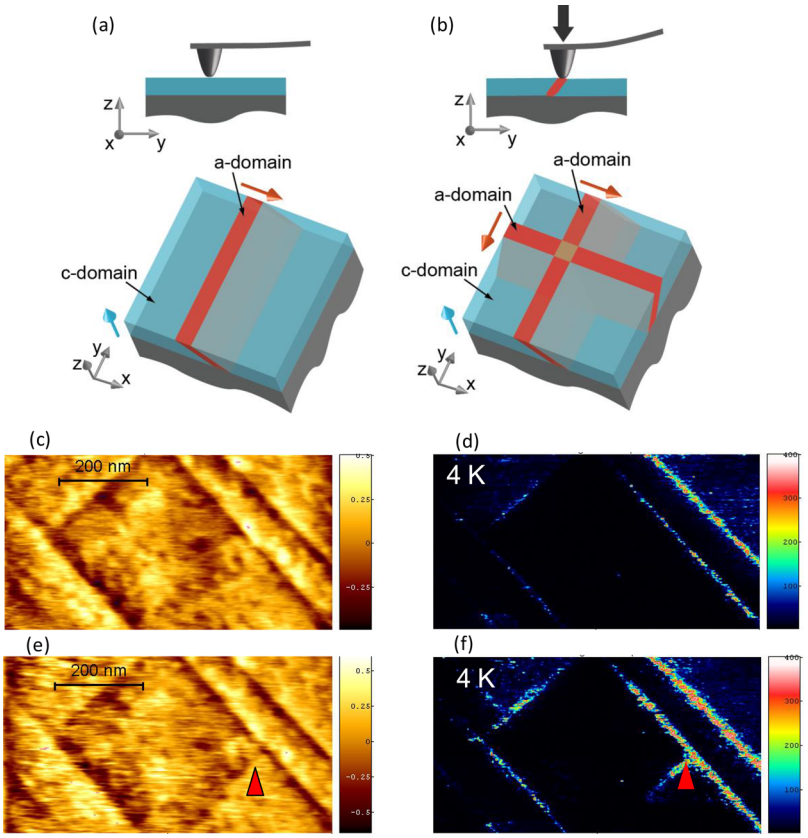

Figure 3. Writing new conductive a-domains by local mechanical pressure applied through the scanning probe. (a) Sketch representing the PZT film with as-grown a-domain. (b) Same area of the PZT film including the new a-domain created by mechanical pressure of the scanning probe. (c,d) Topography and conduction map measured at 4 K under dc tip bias of −7 V on the as-grown film. (e,f) Topography and conduction map measured at 4 K under dc tip bias of −7 V on the same area after the additional scan with zero dc bias and high mechanical force of 250 ± 50 nN applied to the tip. The new a-domain (marked with a red triangle) is signaled by a conductive trace.

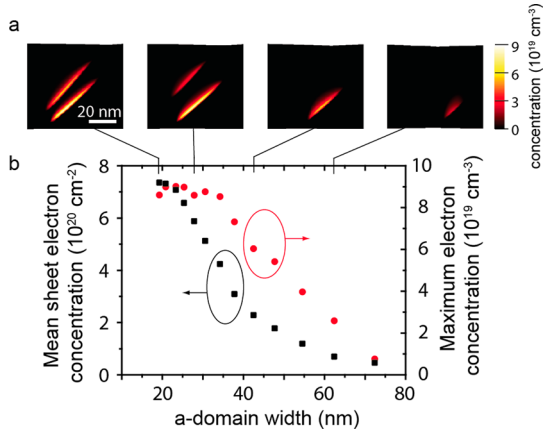

Figure 4. Phase-field calculated electron concentration versus the a-domain width at 50 K. (a) Color scale map of the phase field calculated electron concentration for different a-domain width. (b) Plots of maximum and mean free electron concentration at the a-domain walls versus the a-domain width.

The high-angle annular-dark-field (HAADF) images were recorded with the collection angle ranging from 107 to 200 mrad.

As first-principles calculations[24] indicate, partly charged domain walls in $PbTiO_3$ (which is for this purpose practically identical to PZT (Zr/Ti = 10:90)) are compensated by delocalized electrons at Ti d-states, which changes Ti^{4+} to Ti^{3+}. Thus, an increase of Ti^{3+} concentration at the domain walls can be considered as a signature of conduction by free electrons. EELS data provide evidence for exactly this change at the a-domain boundaries. Figure 5a shows the cross-sectional high-angle annular-dark-field (HAADF) image collected by scanning transmission electron microscopy (STEM) on a 47 nm thick PZT (Zr/Ti = 10:90) film along [100] direction, where two 90° domain walls can be easily identified. The intensity map of Ti-$L_{2,3}$, integrated in an energy window of 455~468 eV is presented in Figure 5b. The subnanometer map in Figure 5b clearly shows strong reduction of intensity signal of Ti-$L_{2,3}$ edge at the domain walls compared to the neighboring domains. The absorption edge profiles for the domain wall plotted together with the data for a- and c-domains (Figure 5c) confirm this trend. The decrease of Ti-$L_{2,3}$ signal intensity (Figure 5c) is consistent with partial change of Ti^{4+} to Ti^{3+}.

In conclusion, nonthermally activated metallic-like conduction was experimentally demonstrated in ubiquitous 90° domain walls of tetragonal PZT films and its origin shown to arise from bending of walls of narrow a-domains due to a controlled interplay between the tetragonality of the film and fine-tuning of its lattice mismatch with the substrate. The demonstrated creation "on demand" of individual stable domains with conduction of this type is another attractive feature for domain circuit engineering. Control of a-domain pattern during growth[20] or by postgrowth in situ writing, erasure, and rewriting by scanning-probe tips and through ultrathin electrodes[25] promise flexibility to our approach. The general character of the demonstrated new concept of metallic-like layer formation at bent domain boundaries implies

DOI: 10.1021/acs.nanolett.5b03450
Nano Lett. 2015, 15, 8049−8055

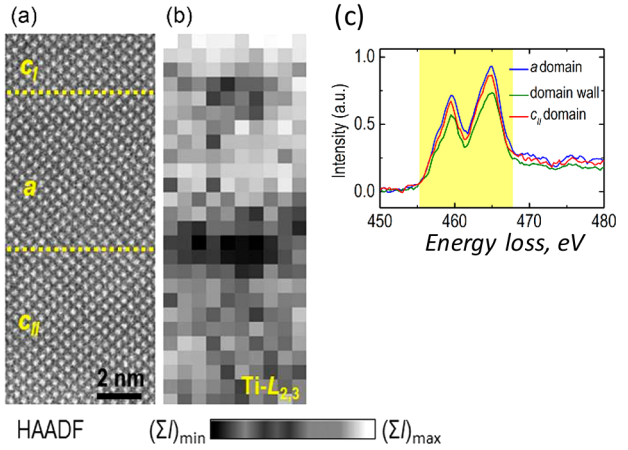

Figure 5. Unit-cell scale scanning transmission electron microscopy (STEM) analysis of the conductive domain walls. (a) High-angle annular-dark field (HAADF) image of 47 nm-thick PZT (Zr/Ti = 10:90) film recorded along [100] direction. Domain walls are marked with yellow dashed lines. (b) Unit-cell scale electron energy-loss spectroscopy (EELS) data measured on the same area. The intensity maps of Ti-$L_{2,3}$ are integrated in an energy window of 455~468 eV. (c) The absorption edge profiles for the domain wall plotted together with the data for the a- and c-domains.

that it can be extended toward functionalization of domain patterns in other ferroelectrics and promises new dimensions to future domain-pattern based circuitry.

■ ASSOCIATED CONTENT

Supporting Information

The Supporting Information is available free of charge on the ACS Publications website at DOI: 10.1021/acs.nanolett.5b03450.

Note 1, Mechanism of elasticity driven rotation of ferroelectric/ferroelastic domain wall; Note 2, Obtaining expression for the energy; Note 3, Sample preparation; Note 4, Domain wall conduction measurements; Note 5, Fine structure of conductive traces at a-domain boundaries; Note 6, Creation of new conductive a-domains by mechanical force; Note 7, The phase-field simulation. (PDF)

■ AUTHOR INFORMATION

Corresponding Author

*E-mail: igor.stolitchnov@epfl.ch. Phone: +41 21 693 4954.

Author Contributions

I.S. conceived and coordinated the study. I.S., L.M., E.C., and A.C. performed scanning force microscopy experiments, L.F. grew the films. T.S. did the phase field simulations. X.K.W. performed the HADDF-STEM and the unit-cell scale EELS measurements. P.Y. and K.S. performed theoretical analysis under guidance of A.K.T., I.S., T.S., and N.S. prepared the manuscript with comments and contributions of all authors. N.S. initiated the study and was responsible for the overall direction.

Notes

The authors declare no competing financial interest.

■ ACKNOWLEDGMENTS

The research leading to these results has received funding from the European Research Council under the EU seventh Framework Program (FP7/2007-2013)/ERC Grant 268058, MOBILE-W and ERC-2013-PoC Grant 620193, MOBILE2DG. The Swiss National Science Foundation (Grants 200020_144454, 200020_156082, and 200020_153177) and the Section for Development and Cooperation of the Swiss Foreign Ministry (Agreement CH-3-SMm-01/02 Swiss-Lithuania cooperation) are acknowledged for additional financial support.

■ REFERENCES

(1) Seidel, J.; Martin, L. W.; He, Q.; Zhan, Q.; Chu, Y. H.; Rother, A.; Hawkridge, M. E.; Maksymovych, P.; Yu, P.; Gajek, M.; Balke, N.; Kalinin, S. V.; Gemming, S.; Wang, F.; Catalan, G.; Scott, J. F.; Spaldin, N. A.; Orenstein, J.; Ramesh, R. Conduction at domain walls in oxide multiferroics. *Nat. Mater.* **2009**, *8*, 229−234.

(2) Maksymovych, P.; Seidel, J.; Chu, Y. H.; Wu, P. P.; Baddorf, A. P.; Chen, L. Q.; Kalinin, S. V.; Ramesh, R. Dynamic Conductivity of Ferroelectric Domain Walls in BiFeO(3). *Nano Lett.* **2011**, *11*, 1906−1912.

(3) Seidel, J.; Maksymovych, P.; Batra, Y.; Katan, A.; Yang, S. Y.; He, Q.; Baddorf, A. P.; Kalinin, S. V.; Yang, C. H.; Yang, J. C.; Chu, Y. H.; Salje, E. K. H.; Wormeester, H.; Salmeron, M.; Ramesh, R. Domain Wall Conductivity in La-Doped BiFeO3. *Phys. Rev. Lett.* **2010**, *105*, 197603.

(4) Guyonnet, J.; Gaponenko, I.; Gariglio, S.; Paruch, P. Conduction at Domain Walls in Insulating Pb(Zr0.2Ti0.8)O3 Thin Films. *Adv. Mater.* **2011**, *23*, 5377.

(5) Farokhipoor, S.; Noheda, B. Conduction through 71 degrees DomainWalls in BiFeO(3) Thin Films. *Phys. Rev. Lett.* **2011**, *107*, 127601.

(6) Meier, D.; Seidel, J.; Cano, A.; Delaney, K.; Kumagai, Y.; Mostovoy, M.; Spaldin, N. A.; Ramesh, R.; Fiebig, M. Anisotropic conductance at improper ferroelectric domain walls. *Nat. Mater.* **2012**, *11*, 284−288.

(7) Eliseev, E. A.; Morozovska, A. N.; Gu, Y. J.; Borisevich, A. Y.; Chen, L. Q.; Gopalan, V.; Kalinin, S. V. Conductivity of twin-domain-wall/surface junctions in ferroelastics: Interplay of deformation potential, octahedral rotations, improper ferroelectricity, and flexoelectric coupling. *Phys. Rev. B: Condens. Matter Mater. Phys.* **2012**, *86*, 085416.

(8) Kalinin, S. V.; Borisevich, A.; Fong, D. Beyond Condensed Matter Physics on the Nanoscale: The Role of Ionic and Electrochemical Phenomena in the Physical Functionalities of Oxide Materials. *ACS Nano* **2012**, *6*, 10423−10437.

(9) Farokhipoor, S.; Noheda, B. Local conductivity and the role of vacancies around twin walls of (001)-BiFeO3 thin films. *J. Appl. Phys.* **2012**, *112*, 052003.

(10) Vasudevan, R. K.; Wu, W. D.; Guest, J. R.; Baddorf, A. P.; Morozovska, A. N.; Eliseev, E. A.; Balke, N.; Nagarajan, V.; Maksymovych, P.; Kalinin, S. V. Domain Wall Conduction and Polarization-Mediated Transport in Ferroelectrics. *Adv. Funct. Mater.* **2013**, *23*, 2592−2616.

(11) Stolichnov, I.; Iwanowska, M.; Colla, E.; Ziegler, B.; Gaponenko, I.; Paruch, P.; Huijben, M.; Rijnders, G.; Setter, N. Persistent conductive footprints of 109° domain walls in bismuth ferrite films. *Appl. Phys. Lett.* **2014**, *104*, 132902.

(12) Strelcov, E.; Kim, Y.; Jesse, S.; Cao, Y.; Ivanov, I. N.; Kravchenko, I. I.; Wang, C. H.; Teng, Y. C.; Chen, L. Q.; Chu, Y. H.; Kalinin, S. V. Probing Local Ionic Dynamics in Functional Oxides at the Nanoscale. *Nano Lett.* **2013**, *13*, 3455−3462.

(13) Maksymovych, P.; Morozovska, A. N.; Yu, P.; Eliseev, E. A.; Chu, Y. H.; Ramesh, R.; Baddorf, A. P.; Kalinin, S. V. Tunable Metallic Conductance in Ferroelectric Nanodomains. *Nano Lett.* **2012**, *12*, 209−213.

(14) Sluka, T.; Tagantsev, A. K.; Damjanovic, D.; Gureev, M.; Setter, N. Enhanced electromechanical response of ferroelectrics due to charged domain walls. *Nat. Commun.* **2012**, *3*, 748.

(15) Sluka, T.; Tagantsev, A. K.; Bednyakov, P.; Setter, N. Free-electron gas at charged domain walls in insulating BaTiO3. *Nat. Commun.* **2013**, *4*, 1808.

(16) Balke, N.; Winchester, B.; Ren, W.; Chu, Y. H.; Morozovska, A. N.; Eliseev, E. A.; Huijben, M.; Vasudevan, R. K.; Maksymovych, P.; Britson, J.; Jesse, S.; Kornev, I.; Ramesh, R.; Bellaiche, L.; Chen, L. Q.;

DOI: 10.1021/acs.nanolett.5b03450
Nano Lett. 2015, 15, 8049−8055

Kalinin, S. V. Enhanced electric conductivity at ferroelectric vortex cores in BiFeO(3). *Nat. Phys.* **2011**, *8*, 81−88.
(17) Crassous, A.; Sluka, T.; Tagantsev, A. K.; Setter, N. Polarization charge as a reconfigurable quasi-dopant in ferroelectric thin films. *Nat. Nanotechnol.* **2015**, *10*, 614.
(18) Vasudevan, R. K.; Morozovska, A. N.; Eliseev, E. A.; Britson, J.; Yang, J. C.; Chu, Y. H.; Maksymovych, P.; Chen, L. Q.; Nagarajan, V.; Kalinin, S. V. Domain Wall Geometry Controls Conduction in Ferroelectrics. *Nano Lett.* **2012**, *12*, 5524−5531.
(19) Gureev, M. Y.; Tagantsev, A. K.; Setter, N. Head-to-head and tail-to-tail 180 degrees domain walls in an isolated ferroelectric. *Phys. Rev. B: Condens. Matter Mater. Phys.* **2011**, *83*, 184104 .
(20) Feigl, L.; Yudin, P.; Stolichnov, I.; Sluka, T.; Shapovalov, K.; Mtebwa, M.; Sandu, C. S.; Wei, X. K.; Tagantsev, A. K.; Setter, N. Controlled stripes of ultrafine ferroelectric domains. *Nat. Commun.* **2014**, *5*, 5677.
(21) Maksymovych, P.; Jesse, S.; Yu, P.; Ramesh, R.; Baddorf, A. P.; Kalinin, S. V. Polarization Control of Electron Tunneling into Ferroelectric Surfaces. *Science* **2009**, *324*, 1421−1425.
(22) Robertson, J.; Warren, W. L.; Tuttle, B. A. Band States and Shallow Hole Traps in Pb(Zr,Ti)O-3 Ferroelectrics. *J. Appl. Phys.* **1995**, *77*, 3975−3980.
(23) Shimada, T.; Ueda, T.; Wang, J.; Kitamura, T. Hybrid Hartree-Fock density functional study of charged point defects in ferroelectric PbTiO3. *Phys. Rev. B: Condens. Matter Mater. Phys.* **2013**, *87*, 174111.
(24) Rahmanizadeh, K.; Wortmann, D.; Bihlmayer, G.; Blugel, S. Charge and orbital order at head-to-head domain walls in PbTiO3. *Phys. Rev. B: Condens. Matter Mater. Phys.* **2014**, *90*, 115104.
(25) Feigl, L.; McGilly, L. J.; Sandu, C. S.; Setter, N. Compliant ferroelastic domains in epitaxial Pb(Zr, Ti)O-3 thin films. *Appl. Phys. Lett.* **2014**, *104*, 172904.

DOI: 10.1021/acs.nanolett.5b03450
Nano Lett. 2015, 15, 8049−8055